

NASA TECHNICAL NOTE



NASA TN D-8220

NASA TN D-8220

LOAN COPY: RETURN TO
AFWL TECHNICAL LIBRARY
KIRTLAND AFB, NM



ANALYSIS OF THE GAS-LUBRICATED FLAT-SECTOR-PAD THRUST BEARING

Izhak Etsion

Lewis Research Center

Cleveland, Ohio 44135



NATIONAL AERONAUTICS AND SPACE ADMINISTRATION • WASHINGTON, D. C. • JUNE 1976



0133779

1. Report No. NASA TN D-8220	2. Government Accession No.	3. Recipient's Catalog No.	
4. Title and Subtitle ANALYSIS OF THE GAS-LUBRICATED FLAT-SECTOR-PAD THRUST BEARING	5. Report Date June 1976		6. Performing Organization Code
	7. Author(s) Izhak Etsion		8. Performing Organization Report No. E-8623
9. Performing Organization Name and Address Lewis Research Center National Aeronautics and Space Administration Cleveland, Ohio 44135	10. Work Unit No. 505-04		11. Contract or Grant No.
	12. Sponsoring Agency Name and Address National Aeronautics and Space Administration Washington, D.C. 20546		13. Type of Report and Period Covered Technical Note
15. Supplementary Notes		14. Sponsoring Agency Code	
16. Abstract A flat sector-shaped pad geometry for a gas-lubricated thrust bearing is analyzed considering both the pitch and roll of the pad. It is shown that maximum load capacity is achieved when the pad is tilted so as to create uniform minimum film thickness along the pad trailing edge. Performance characteristics for various geometries and operating conditions of gas thrust bearings are presented in the form of design curves, and a comparison is made with the rectangular slider approximation. It is found that this approximation is unsafe for practical design, since it always overestimates load capacity.			
17. Key Words (Suggested by Author(s)) Bearings Gas bearings Thrust bearings		18. Distribution Statement Unclassified - unlimited STAR category 37	
19. Security Classif. (of this report) Unclassified	20. Security Classif. (of this page) Unclassified	21. No. of Pages 29	22. Price* \$4.00

ANALYSIS OF THE GAS-LUBRICATED FLAT-SECTOR-PAD

THRUST BEARING

by Izhak Etsion*

Lewis Research Center

SUMMARY

A flat sector-shaped pad geometry for a gas-lubricated thrust bearing is analyzed considering both the pitch and roll of the pad. The analysis uses only two parameters (rather than the conventional four) to completely describe pad pitch and roll about a certain point. This was achieved by transforming the pitch and roll about the point to a corresponding pure pitch about a certain radial pivot line. This enables performance optimization to be based on the true geometry. Maximum load capacity is achieved when the pad is tilted so as to create uniform minimum film thickness along the pad trailing edge. Performance characteristics for sector angles of 30° , 45° , and 60° and radius ratios of 0.3, 0.5, and 0.7 are presented, over the range from almost incompressible lubrication to a compressibility number as high as 100. A comparison is made with the rectangular approximation. It is found that this approximation is unsafe for practical design, since it always overestimates load capacity.

INTRODUCTION

Of all the existing thrust bearing configurations the flat sector pad (fig. 1) is the simplest to produce and probably the most commonly used for practical applications. It is therefore astonishing to find that so little has been published in the literature on this sort of bearing.

Taylor and Saffman (ref. 1) present an analytical solution for a flat circular plate misaligned about a radial line and spinning opposite a fixed stator disk that is perpendicular to the axis of rotation. Although the actual film thickness distribution in the

* National Research Council - National Aeronautics and Space Administration Research Associate.

lubricating film was used, the solution is inapplicable to thrust bearings that consist of individual flat sector pads. While for the circular plate the film is converging-diverging, for the sector pad it is usually wholly converging. Gross (ref. 2) in his book presents a solution, in the form of an infinite series, for a sector pad with exponential film thickness distribution. An approximate solution then follows in which he assumes that the film thickness is independent of radius. This type of bearing, known as a Michell bearing, is by no means an actual flat sector pad. For a flat sector pad tilted about any point the clearance varies in both the radial and circumferential directions, with the circumferential variation being sinusoidal rather than linear.

In two other references (refs. 3 and 4) the sector-shaped pad is approximately by a rectangular slider. The transformation from a sector shape is made by assuming that the rectangular width is equal to the mean circumference of the sector and that the length is equal to the difference between the inner and outer radii. This approximation not only distorts the sector shape, but also introduces linear film thickness and velocity profiles that are independent of radius.

Extensive work on pad bearings has been done by Shapiro and Colsher (ref. 5). They investigated the crowned sector pad and included optimization criteria, design information, and procedures. The flat pad was treated as a particular case of zero crown height. Although the problem was generally posed, solutions were limited to a pad inclined about a radial line through the center of the pad.

In the course of developing a new type of gas-lubricated thrust bearing (ref. 6), it was found that solutions that cover a wide range of flat-sector-pad operating conditions are desired. Such solutions are not available in the open literature. It is the intent of this report to provide the necessary data for design of flat-sector-pad configurations. A solution will be sought for bearings of various pad sector angles and radius ratios operating over a wide range of compressibility numbers. Bearing load capacity, center-of-pressure location, and friction loss will be given.

ANALYSIS

Film Thickness Distribution

One reason for approximating the sector-shaped pad as a rectangular slider is the large number of parameters involved in the exact solution. The film thickness distribution for a tilted pad is defined by four parameters. Two of them describe the location of the pivot, while the other two measure the amount of tilt about radial and tangential lines through the pivot point, referred to as pitch and roll.

Figure 2 shows a flat sector pad tilted about some point O' with a pitch α_r and

roll α_θ . (All symbols are defined in the appendix.) If the pad is initially parallel to some plane at a distance h'_O , the expression for the clearance at any point (r, θ) is

$$h = h'_O + \alpha_r r \sin(\theta' - \theta) + \alpha_\theta [r' - r \cos(\theta' - \theta)] \quad (1)$$

Using the clearance at the center O as a reference, we have

$$h = h_O + \alpha_r r \sin(\theta' - \theta) - \alpha_\theta r \cos(\theta' - \theta)$$

where

$$h_O = h'_O + r' \alpha_\theta \quad (2)$$

A radial line at an angle θ_p can now be found along which the clearance is constant and equal to h_O . This radial pivot line is defined by the equation

$$\alpha_r r \sin(\theta' - \theta_p) - \alpha_\theta r \cos(\theta' - \theta_p) = 0$$

where the angle θ_p is given by

$$\tan(\theta' - \theta_p) = \frac{\alpha_\theta}{\alpha_r} \quad (3)$$

The pitch about the pivot line is

$$\gamma = -\frac{1}{r} \left(\frac{dh}{d\theta} \right)_{\theta=\theta_p} = \alpha_r \cos(\theta' - \theta_p) + \alpha_\theta \sin(\theta' - \theta_p) \quad (4)$$

The preceding analysis shows that any tilt about some given point is equivalent to a pure pitch about a certain radial line. This can be easily understood by visualizing a plane parallel to the runner that goes through the origin of the sector (point O in fig. 2). The radial pivot line is the intersection between this parallel plane and the plane of the tilted sector. Equations (3) and (4) represent the proper transformation. By considering the clearance h_O along this pivot line as a reference, we can give the film thickness at any point (r, θ) by

$$h = h_O + \gamma r \sin(\theta_p - \theta) \quad (5)$$

where γ is the amount of tilt about the pivot line.

Describing the film thickness distribution in terms of θ_p and γ reduces the number of involved parameters from four in equation (1) to two in equation (5). We normalize the clearance by h_o and the radial coordinate by the outer radius r_o . The nondimensional film thickness then becomes

$$H = 1 + \epsilon R \sin(\theta_p - \theta) \quad (6)$$

where

$$\epsilon = \gamma \frac{r_o}{h_o}$$

$$R = \frac{r}{r_o}$$

It will be instructive, prior to obtaining explicit solutions, to examine equation (5) in order to understand some features of the flat pad. When dealing with an actual flat pad, the location θ_p of the pivot line plays an important role in regard to the convergence or divergence of the fluid film. Differentiating equation (5) yields the circumferential and radial gradients

$$\frac{1}{r} \frac{dh}{d\theta} = -\gamma \cos(\theta_p - \theta) \quad (7a)$$

$$\frac{dh}{dr} = \gamma \sin(\theta_p - \theta) \quad (7b)$$

From this we can see that whenever $\gamma > 0$ the condition for circumferential clearance convergence is

$$-\frac{\pi}{2} < \theta_p - \theta < \frac{\pi}{2}$$

To meet this demand for any θ within the pad boundaries,

$$\theta_{\max} - \frac{\pi}{2} < \theta_p < \frac{\pi}{2} + \theta_{\min}$$

and since $\theta_{\max} = \beta$ and $\theta_{\min} = 0$ we have

$$\beta - \frac{\pi}{2} < \theta_p < \frac{\pi}{2} \quad (8)$$

The range of pivot location for circumferential film thickness variation as described by expression (8) can be divided into three different regions corresponding to three different modes of radial clearance variation (fig. 3).

Region a: $\beta - \pi/2 < \theta_p < 0$. - In this region the pivot line is ahead of the leading edge. For any θ within the pad, $\theta_p - \theta < 0$. Hence, from equation (7b) it is clear that radial convergence exists all over the pad.

The maximum and minimum clearances are at the points $(r_i, 0)$ and (r_o, β) , respectively, and the clearance ratio is

$$\frac{h_1}{h_2} = \frac{1 + \epsilon \frac{r_i}{r_o} \sin \theta_p}{1 + \epsilon \sin(\theta_p - \beta)} \quad (9a)$$

Note that region a can exist only for $\beta < \pi/2$.

Region b: $0 \leq \theta_p \leq \beta$. - For any $\theta > \theta_p$ the film thickness still converges radially, but the portion of the pad between the leading edge and the pivot line ($\theta < \theta_p$) assumes radial divergence. The maximum and minimum clearances are at $(r_o, 0)$ and (r_o, β) , respectively. The clearance ratio is

$$\frac{h_1}{h_2} = \frac{1 + \epsilon \sin \theta_p}{1 + \epsilon \sin(\theta_p - \beta)} \quad (9b)$$

Region c: $\beta < \theta_p < \pi/2$. - Here, radial divergence exists over the entire pad. The minimum clearance occurs at (r_i, β) , the maximum clearance occurs at $(r_o, 0)$, and the clearance ratio is

$$\frac{h_1}{h_2} = \frac{1 + \epsilon \sin \theta_p}{1 + \epsilon \frac{r_i}{r_o} \sin(\theta_p - \beta)} \quad (9c)$$

Solution of the Reynolds Equation

For isothermal films the compressible Reynolds equation in polar coordinates is

$$\frac{\partial}{\partial r} \left(\frac{rph^3}{\mu} \frac{\partial p}{\partial r} \right) + \frac{1}{r} \frac{\partial}{\partial \theta} \left(\frac{ph^3}{\mu} \frac{\partial p}{\partial \theta} \right) = 6r\omega \frac{\partial(ph)}{\partial \theta} \quad (10)$$

To transform equation (10) into dimensionless form, the following substitutions are used:

$$\begin{aligned} R &= \frac{r}{r_0} \\ P &= \frac{p}{p_a} \\ H &= \frac{h}{h_0} \\ \Lambda &= \frac{6\mu\omega r_0^2}{p_a h_0^2} \end{aligned}$$

With these transformations the Reynolds equation becomes

$$\frac{\partial}{\partial R} \left(H^3 R P \frac{\partial P}{\partial R} \right) + \frac{1}{R} \frac{\partial}{\partial \theta} \left(H^3 P \frac{\partial P}{\partial \theta} \right) = \Lambda H_0^2 R \frac{\partial}{\partial \theta} (PH) \quad (11)$$

The boundary conditions are $P = 1$ on the boundaries of the pad.

Equation (11) can be written in terms of the variable Q , where $Q = (PH)^2$ (ref. 7):

$$\frac{\partial}{\partial R} \left[R \left(\frac{H}{2} \frac{\partial Q}{\partial R} - Q \frac{\partial H}{\partial R} \right) \right] + \frac{1}{R} \frac{\partial}{\partial \theta} \left(\frac{H}{2} \frac{\partial Q}{\partial \theta} - Q \frac{\partial H}{\partial \theta} \right) = \frac{\Lambda H_0^2 R}{2\sqrt{Q}} \frac{\partial Q}{\partial \theta} \quad (12)$$

We now differentiate the left side and rearrange, noting that for the film thickness distribution as given by equation (6),

$$\frac{\partial^2 H}{\partial R^2} = 0$$

and

$$\frac{\partial H}{\partial R} + \frac{1}{R} \frac{\partial^2 H}{\partial \theta^2} = 0$$

The Reynolds equation then becomes

$$\frac{\partial^2 Q}{\partial R^2} + \frac{1}{R^2} \frac{\partial^2 Q}{\partial \theta^2} - \left[\frac{\partial}{\partial R} \left(\ln \frac{H}{R} \right) \right] \frac{\partial Q}{\partial R} - \left[\frac{1}{R^2} \frac{\partial}{\partial \theta} \left(\ln \frac{H}{R} \right) \right] \frac{\partial Q}{\partial \theta} = \frac{\Lambda H_2^2}{H\sqrt{Q}} \frac{\partial Q}{\partial \theta} \quad (13)$$

Equation (13) is expanded by finite differences and solved numerically by using the Gauss-Seidel iteration method. After the pressure distribution is known, the total load capacity is obtained from

$$\bar{W} = \frac{W}{p_a r_o^2} \int_{r_i/r_o}^1 \int_0^\beta (P - 1) R \, d\theta \, dR \quad (14)$$

The pad area is given by

$$A = \frac{\beta}{2} (r_o^2 - r_i^2) = \frac{1}{2} \beta r_o^2 \left[1 - \left(\frac{r_i}{r_o} \right)^2 \right]$$

and the nondimensional unit load of the bearing is

$$\frac{W}{p_a A} = \frac{\bar{W}}{\beta \left[1 - \left(\frac{r_i}{r_o} \right)^2 \right]} \quad (15)$$

The nondimensional radial and angular coordinates of the center of pressure are given by

$$R_{cp} = \frac{1}{W} \int_{r_i/r_o}^1 \int_0^\beta (P - 1) R^2 \, d\theta \, dR \quad (16a)$$

$$\sin \theta_{cp} = \frac{1}{WR_{cp}} \int_{r_i/r_o}^1 \int_0^\beta (P - 1) R^2 \sin \theta \, d\theta \, dR \quad (16b)$$

The shear stress on the runner is

$$\tau = \frac{\mu \omega r}{h} + \frac{h}{2r} \frac{\partial p}{\partial \theta}$$

and the power loss is

$$F = \iint \tau \omega R^2 d\theta dR$$

Defining

$$\bar{F} = \frac{F}{p_a h_2 \omega r_o^2}$$

gives

$$\bar{F} = \frac{1}{H_2} \int_{r_i/r_o}^1 \int_0^\beta \left(\frac{\Lambda H_2^2}{6} \frac{R^3}{H} + \frac{HR}{2} \frac{\partial P}{\partial \theta} \right) d\theta dR \quad (17)$$

The previous equations are for one pad. When multiple pads are considered, each pad is handled separately and the results added.

RESULTS

Optimum Pivot Location and Bearing Performance

In total, 12 different geometries were analyzed. Inner to outer radius ratios were 0.3, 0.5, and 0.7 at pad angles of 30° , 45° , 60° , and 90° . Each pad was run at compressibility numbers from 1 to 100 with various pivot locations. Performance characteristics such as unit load, center-of-pressure location, and power loss were found as a function of clearance ratio and pivot location. Figure 4 is a typical plot describing unit load variation. Two important results are the existence of an optimum clearance ratio for maximum unit load and the effect of pivot location on the load capacity. The highest unit load is achieved when the radial pivot line is placed at the pad trailing edge. By shifting the pivot line from the leading to the trailing edge, the maximum available unit load for the particular pad of figure 4 is increased by 55 percent. In figure 5 the maximum available unit load of four different pads is plotted against pivot location. Figure 5(a) presents the low compressibility range ($\Lambda = 10$), while figure 5(b) is for $\Lambda = 100$. It is clear that for the whole range of pad angles and operating conditions there is a sharp maximum at the pivot location $\theta_p/\beta = 1$. The same results were obtained for the other radius ratios. Thus, to get the maximum load capacity

from a given pad, the pad should be tilted in a way that maintains a uniform minimum film thickness along the trailing edge.

A physical explanation for this is that the pressure buildup in the lubricating film is affected by the resistance to lubricant outflow. Some of this flow occurs along the inner and outer circumferences of the pad, but the larger portion leaks across the trailing edge. Hence it would be advantageous to decrease the escape area along this boundary. For the three regions of pivot location discussed in the analysis and for a given minimum film thickness h_2 , the lowest escape area and hence the highest pressure buildup can be achieved by placing the pivot line on the trailing edge.

To examine the effect of pad geometry on load capacity, maximum available unit loads at $\theta_p/\beta = 1$ are presented in table I. The highest load is achieved at the lowest radius ratio. This means that for a given outer radius the lowest possible inner radius is desirable. Low radius ratio not only produces high unit load but further increases the load capacity by providing larger bearing area. From table I it is seen that at radius ratios of 0.7 the best bearing configuration of those computed is that consisting of 12 pads of 30° each. The gain in maximum load capacity over the next best configuration, having $\beta = 45^\circ$, is about 20 percent.

At a radius ratio of 0.5 there is only a slight difference between the 30° and 45° pads. At $r_i/r_o = 0.3$ the 60° pad is slightly better than the 45° up to $\Lambda = 10$ and gives 16 percent more load capacity than the 30° configuration. At higher compressibilities, up to $\Lambda = 100$, the 45° pad takes over, being slightly better than the 60° at $\Lambda = 25$ and $\Lambda = 50$ and giving 11 and 7.5 percent more load than the 30° pad at $\Lambda = 25$ and $\Lambda = 50$, respectively. At $\Lambda = 100$ the maximum available load of the 30° and 60° pads is the same, being only 4 percent less than that of the 45° pad.

Figures 6 to 10 present performance characteristics as functions of the clearance parameter for $\theta_p/\beta = 1$ and various compressibility numbers. Note that for $\theta_p/\beta = 1$, $h_o = h_2$. Hence the clearance parameter is $\epsilon = \gamma r_o/h_2$. The clearance parameter ϵ is considered to be more convenient for bearing construction than the film thickness ratio h_1/h_2 . Equation (9b) gives the relation between h_1/h_2 and ϵ . Pad angles of 30° and 45° are considered, with the addition of the 60° pad at $r_i/r_o = 0.3$. From figures 6(a) to (c) it can be seen that although at $r_i/r_o = 0.3$ and $\Lambda < 25$ the maximum available load capacity is achieved at $\beta = 60^\circ$, the maximum load region is confined to a narrow range of clearance parameter, compared with the 30° or 45° configurations. On the other hand, the 60° pad is advantageous because a smaller number of pads are required.

From figures 6(d) to (g) it is seen that for $r_i/r_o = 0.5$, like in the case of $r_i/r_o = 0.3$, again the 30° pad has a wider range of clearance parameter around the maximum unit load. As a general rule the optimum pad angle decreases as the radius ratio and compressibility number increase. The optimum pad angle also appears to be that

which results in a pad having a mean circumferential length approximately equal to $r_o - r_i$, that is, a "square" pad.

In figures 7 to 9, the angular location of the center of pressure is presented. For all cases there is only a slight change with clearance parameter variation. This change is most pronounced at low compressibility numbers and decreases to less than 5 percent at $\Lambda = 100$. Loci of maximum load capacity are also shown; this information will be useful for tilting pad design.

Radial location of the center of pressure is much less sensitive to clearance parameter variation, and values to cover the whole range of operating conditions within an accuracy of 2 percent are given in table II. For a radius ratio of 0.7 the center of pressure is very close to the midradius of the pad. The center of pressure moves toward the outside as the radius ratio and pad angle decrease.

Figure 10 presents power loss coefficients for the various geometries and operating conditions. Power loss is shown in the form $F/W\omega h_2$; thus the lower the value of $F/W\omega h_2$ the higher the bearing efficiency. Around the values of clearance parameter for maximum load the power loss coefficient is not much affected by changes in the compressibility number for Λ up to 50. The efficiency drops at higher compressibility numbers, being about 20 percent less at $\Lambda = 100$ than at $\Lambda = 1$. Pad angle β affects the efficiency similar to the way it affects the unit load. Hence, high efficiency is related to high load capacity. Again, the low radius ratio of 0.3 is the most efficient. This, combined with its higher load capacity, makes the low radius ratio a desirable feature in bearing design.

Comparison with Rectangular Approximation

Most of the published performance information on tilted-pad thrust bearings is for rectangular sliders. The approximation of a sector shape is made by assuming that the rectangular length is equal to the difference between the inner and outer radii of the sector and that the width and velocity are equal to the mean circumferential length and velocity of the sector. The equivalent compressibility number Λ_R of the rectangular approximation becomes

$$\Lambda_R = \beta \left[\frac{1 + \left(\frac{r_i}{r_o}\right)}{2} \right]^2 \Lambda$$

The sector-pad analysis of reference 5 was based on a pad inclination about a radial line through the center of the pad ($\theta_p/\beta = 0.5$). This is the most common technique in sector-pad bearing analyses and is based on the assumption that it best fits the rectangular approximation. However, as will now be shown this is not the case.

Table III compares the variation in unit load, at various clearance ratios, for two sector-shaped pads and their rectangular approximations. The first sector pad, having a radius ratio of 0.9, a pad angle of 24° , and a compressibility number of 26.5, corresponds to a rectangular slider with a length-width ratio of 0.25 and an equivalent compressibility number of 10. The second sector pad has $r_i/r_o = 0.3$, $\beta = 62^\circ$ and $\Lambda = 22$ and is approximated by a rectangular slider having $L/B = 1$ and $\Lambda_R = 10$.

As can be seen from table III, the rectangular approximation always overestimates the unit load. The error increases as r_i/r_o and θ_p/β become less than unity. For pad 1, having $r_i/r_o = 0.9$ and $\theta_p/\beta = 1$, the results differ by less than 3 percent (when $h_1/h_2 \leq 3$); but the difference is 11 percent for $\theta_p/\beta = 0.5$. For pad 2, having $r_i/r_o = 0.3$, which is a more practical ratio than $r_i/r_o = 0.9$, the rectangular approximation overestimates the load by 12 to 35 percent for $\theta_p/\beta = 1$ and by as much as 60 percent when $\theta_p/\beta = 0.5$. The unit load for the rectangular approximation was reproduced from reference 8, and the close agreement with the results for pad 1 serves as a check on the validity of the present analysis.

Another error resulting from the rectangular approximation is the center-of-pressure location. The rectangular approximation assumes the midradius of the pad as the center-of-pressure location, thus producing errors as large as 10 percent of the pad length (see table II).

CONCLUDING REMARKS

The flat sector-shaped pad was analyzed by taking into account both the pitch and roll of the pad. The highest load capacity is achieved when the pad is tilted about its trailing edge, and for most operating conditions the best bearing configuration is that with a low radius ratio. The optimum pad angle depends on the radius ratio and compressibility number.

Errors resulting from the rectangular approximation were pointed out. These are overestimation of load capacity and mislocation of the center of pressure. Design curves for actual sector-shaped pads were presented to provide bearing unit load, center-of-pressure location, and power loss for various radius ratios, pad angles,

and a wide range of operating conditions from almost incompressible lubrication to compressibility numbers as high as 100.

Lewis Research Center,
National Aeronautics and Space Administration,
Cleveland, Ohio, March 29, 1976,
505-04.

APPENDIX - SYMBOLS

A	pad area, $\beta(r_o^2 - r_i^2)/2$
B	width of rectangular slider
F	power loss
\overline{F}	nondimensional power loss, $F/p_a \omega h_2 r_o^2$
H	nondimensional film thickness, h/h_o
h	film thickness
h_o	film thickness along pivot line
h'_o	film thickness at point where pad is tilted
h_1, h_2	maximum and minimum film thicknesses
L	length of rectangular slider (normal to direction of motion)
P	nondimensional pressure, p/p_a
p	pressure
p_a	ambient pressure
Q	$(PH)^2$
R	nondimensional radius, r/r_o
R_{cp}	nondimensional radius to center of pressure, r_{cp}/r_o
r	radial coordinate
r_{cp}	radius to center of pressure
r_i	pad inner radius
r_o	pad outer radius
r'	radius to point where pad is tilted
W	pad load capacity
\overline{W}	nondimensional load, $W/p_a r_o^2$
α_r	tilt about a radial line (pitch)
α_θ	tilt about a tangent line (roll)
β	angular extent of pad
ϵ	clearance parameter, $\gamma r_o/h_o$

γ	pitch about pivot line
θ	angular coordinate, measured from leading edge
θ'	angle to point where pad is tilted
θ_{cp}	angle to center of pressure
θ_p	angle to pivot line
Λ	compressibility number, $6\mu\omega r_o^2/p_a h_2^2$
Λ_R	equivalent compressibility number for rectangular approximation
μ	viscosity
τ	shear stress on runner
ω	shaft speed

REFERENCES

1. Taylor, G.; and Saffman, P. G.: Effects of Compressibility at Low Reynolds Number. *J. Aero. Sci.*, vol. 24, no. 8, 1957, pp. 553-562.
2. Gross, William A.: Gas Film Lubrication. Ch. 4, John Wiley & Sons, Inc., 1962, pp. 142-254.
3. Rieger, N. F., ed.: Design of Gas Bearings. Volume 1: Design Notes. Rensselaer Polytechnic Inst. and Mech. Tech., Inc., 1966.
4. Constantinescu, V. N.: Gas Lubrication. Ch. 7, Am. Soc. Mech. Engrs., 1969, pp. 422-516.
5. Shapiro, W.; and Colsher, R.: Analysis and Performance of the Gas-Lubricated Tilting Pad Thrust Bearing. *Am. Soc. Lubric. Engrs. Trans.*, vol. 12, no. 3, Dec. 1969, pp. 206-215.
6. Anderson, W. J.: Analysis of an All-Metallic Resilient Pad Gas-Lubricated Thrust Bearing. *J. Lubric. Tech., ASME Trans.*, vol. 97, no. 2, Apr. 1975, pp. 296-302.
7. Castelli, V.; and Pirvics, J.: Review of Numerical Methods in Gas Bearing Film Analysis. *J. Lubric. Tech., ASME Trans.*, vol. 90, Oct. 1968, pp. 777-792.
8. Pinkus, Oscar; and Sternlicht, Beno: Theory of Hydrodynamic Lubrication. McGraw-Hill Book Co., Inc., 1961, p. 143.

TABLE I. - MAXIMUM AVAILABLE UNIT LOAD FOR VARIOUS GEOMETRIES AND
COMPRESSIBILITY NUMBERS

[Pivot location, θ_p/β , 1.]

Compressibility number, Λ	Ratio of pad inner radius to outer radius, r_i/r_o											
	0.3				0.5				0.7			
	Angular extent of pad, β , deg											
	30	45	60	90	30	45	60	90	30	45	60	90
	Maximum available unit load, $(W/p_a A)_{\max} \times 10^3$											
1	4.1	4.7	4.8	4.3	4.1	4.2	3.8	3	2.8	2.3	1.9	1.4
10	41	46	47	40	40	41	37	28	28	23	19	14
25	97	108	107	91	95	95	87	66	66	55	46	32
50	172	185	182	151	170	166	150	114	122	102	85	60
100	283	295	282	229	276	266	239	181	204	172	145	103

TABLE II. - RADIAL LOCATION OF CENTER OF PRESSURE
FOR VARIOUS GEOMETRIES AND COMPRESSIBILITY NUMBERS

[Pivot location, θ_p/β , 1; values are for optimum load capacity.]

Compressibility number, Λ	Ratio of pad inner radius to outer radius, r_i/r_o						
	0.3			0.5		0.7	
	Angular extent of pad, β , deg						
	30	45	60	30	45	30 and 45	
	Radial location of center of pressure, r_{cp}/r_o						
1 to 25	0.723	0.705	0.695	0.773	0.767	0.854	
50	.722	.702	.692	.773	.767	.854	
100	.716	.702	.690	.771	.766	.854	

TABLE III. - COMPARISON BETWEEN UNIT LOAD FOR FLAT
SECTOR-SHAPED PADS AND THEIR RECTANGULAR APPROXIMATION

Clearance ratio, h_1/h_2	Pad 1 ^a			Pad 2 ^b		
	Pivot location, θ_p/β		Rectangular approxima- tion (ref. 9)	Pivot location, θ_p/β		Rectangular approxima- tion (ref. 9)
	0.5	1		0.5	1	
	Unit load, $(W/P_a A) \times 10^2$					
1.5	1.122	1.152	1.167	5.301	5.686	7.717
1.8	1.355	1.409	1.432	6.505	7.488	9.613
2.0	1.436	1.505	1.528	6.884	8.272	10.287
2.2	1.482	1.565	1.575	7.049	8.816	10.683
2.5	1.509	1.612	1.633	7.046	9.307	10.908
2.8	1.507	1.625	1.657	6.868	9.527	10.887
3.0	1.495	1.623	1.660	6.696	9.571	10.753
4.0	1.381	1.544	1.613	5.648	9.148	9.613
5.0	1.246	1.429	1.535	4.676	8.334	8.390

^aRatio of pad inner radius to outer radius, r_i/r_o , 0.9; angular extent of pad, β , 24° ; compressibility number, Λ , 26.5.

^b $r_i/r_o = 0.3$; $\beta = 62^\circ$; $\Lambda = 22$.

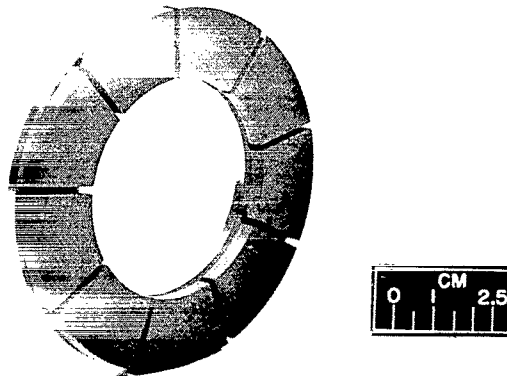


Figure 1. - Sector-pad thrust bearing.

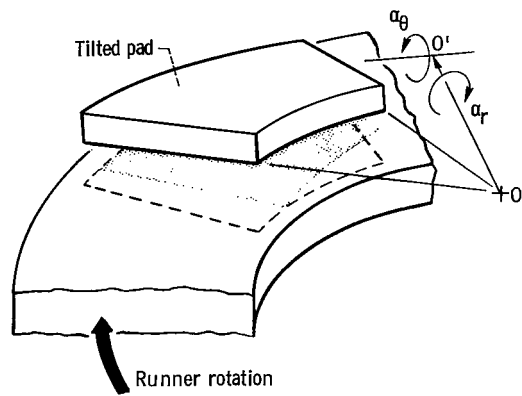
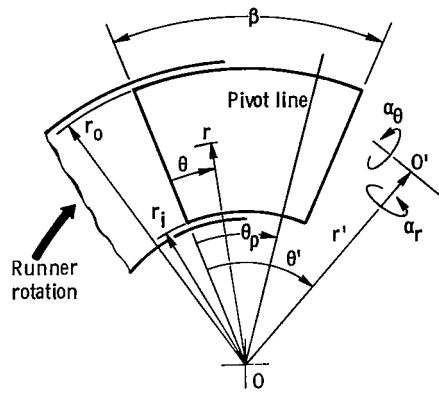


Figure 2. - Geometry of sector pad.

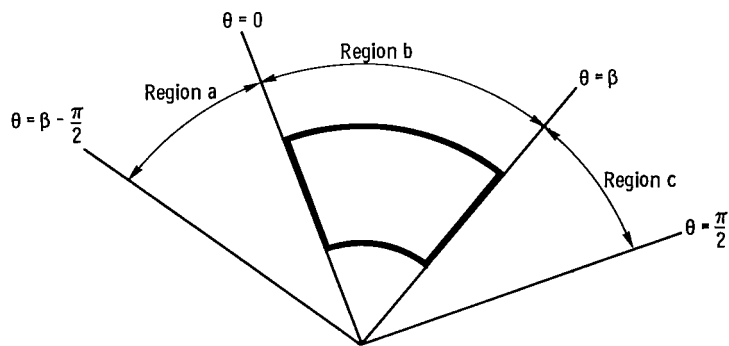


Figure 3. - Different regions of pivot-line location.

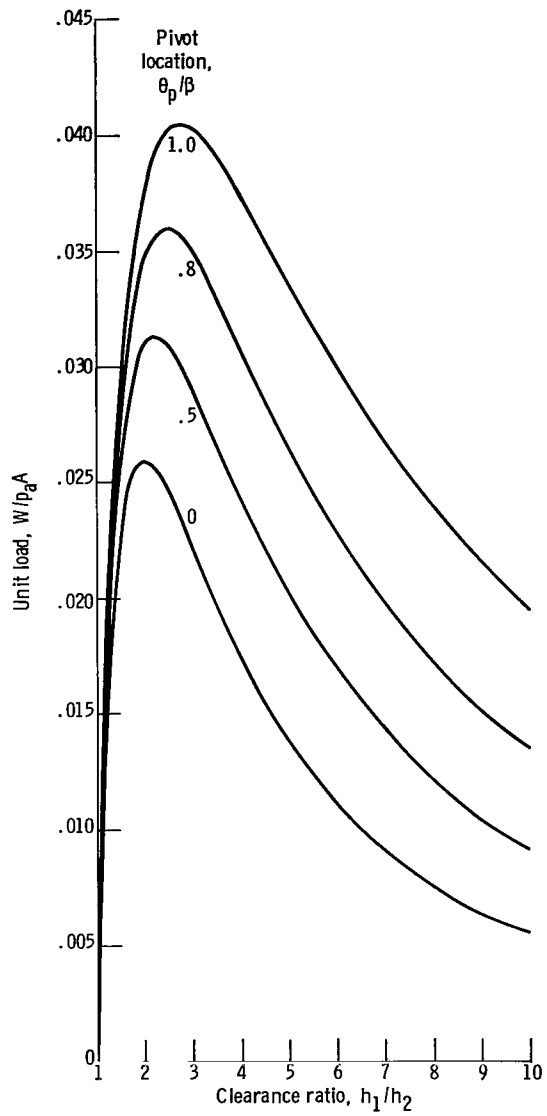


Figure 4. - Unit load at various pivot locations.
 Ratio of pad inner radius to outer radius,
 r_1/r_0 , 0.5; angular extent of pad, β , 45° ; com-
 pressibility number, Λ , 10.

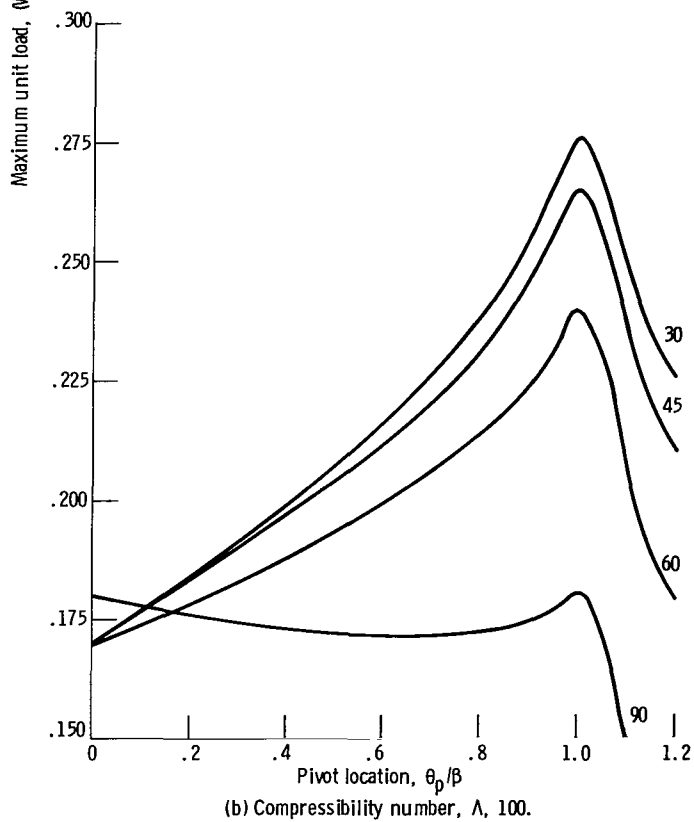
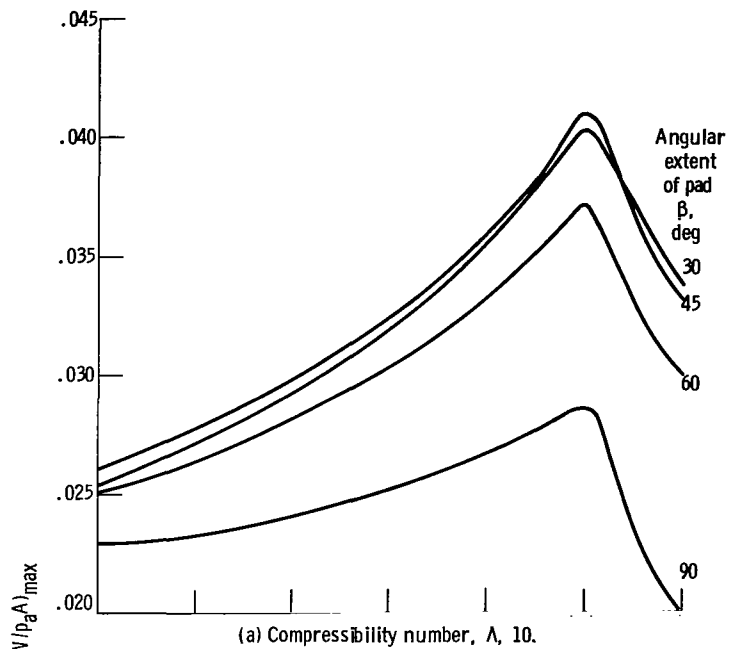


Figure 5. - Maximum available unit load at various pad angles for low and high compressibility numbers. Ratio of pad inner radius to outer radius, r_i/r_o , 0.5.

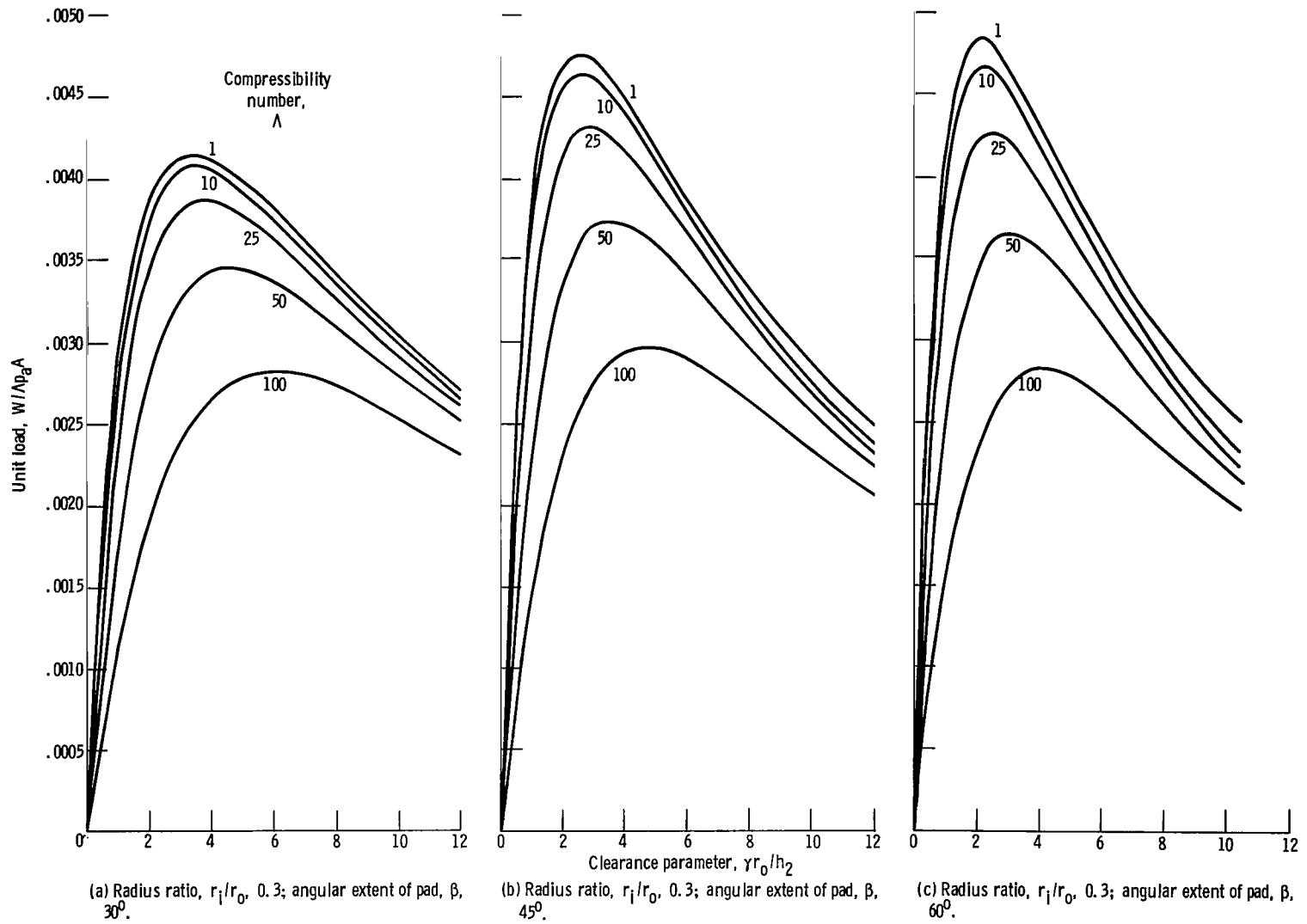


Figure 6. - Unit load for optimally tilted pad for various radius ratios and angular extents of pad, at various compressibility numbers.

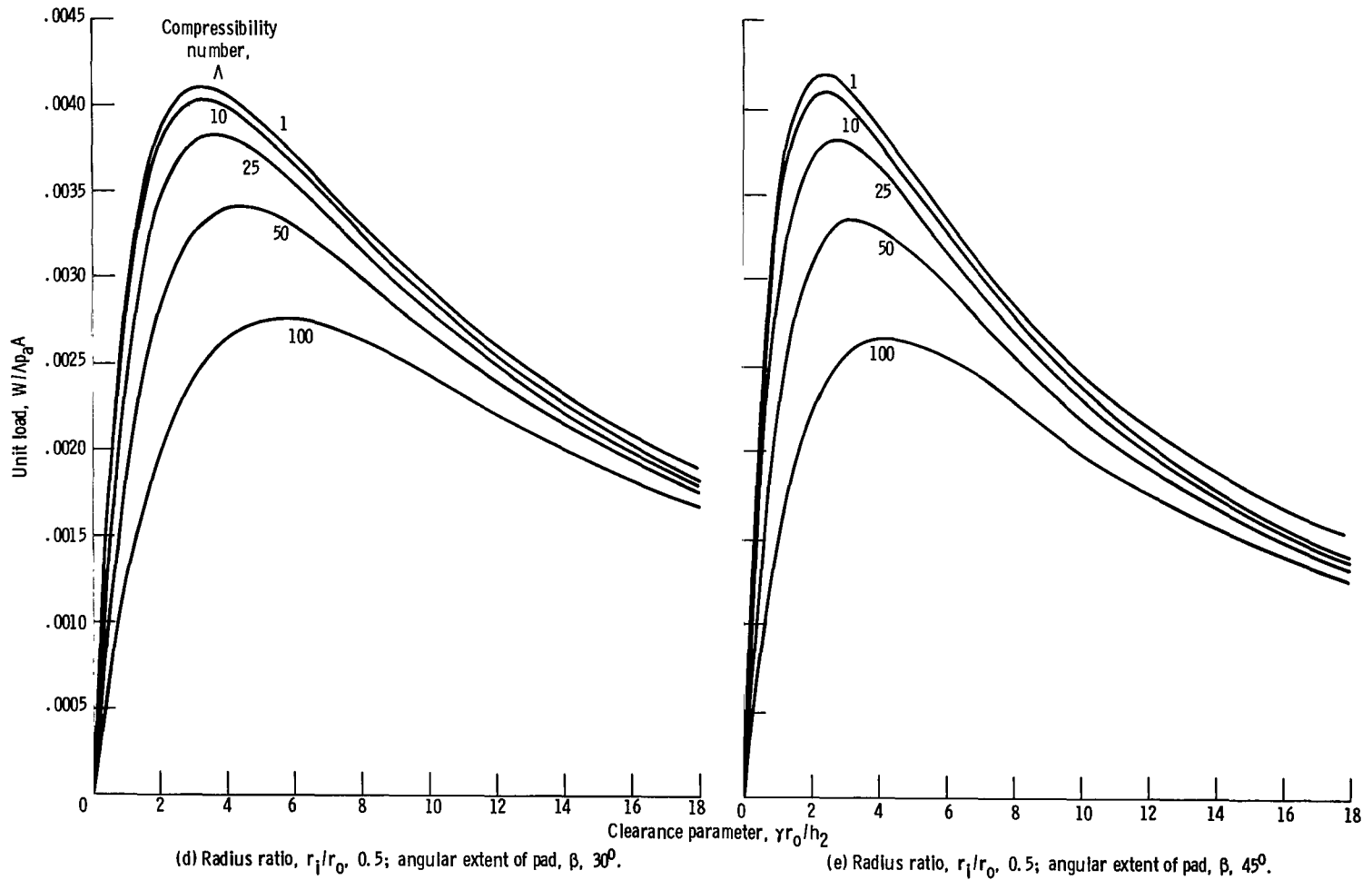


Figure 6. - Continued.

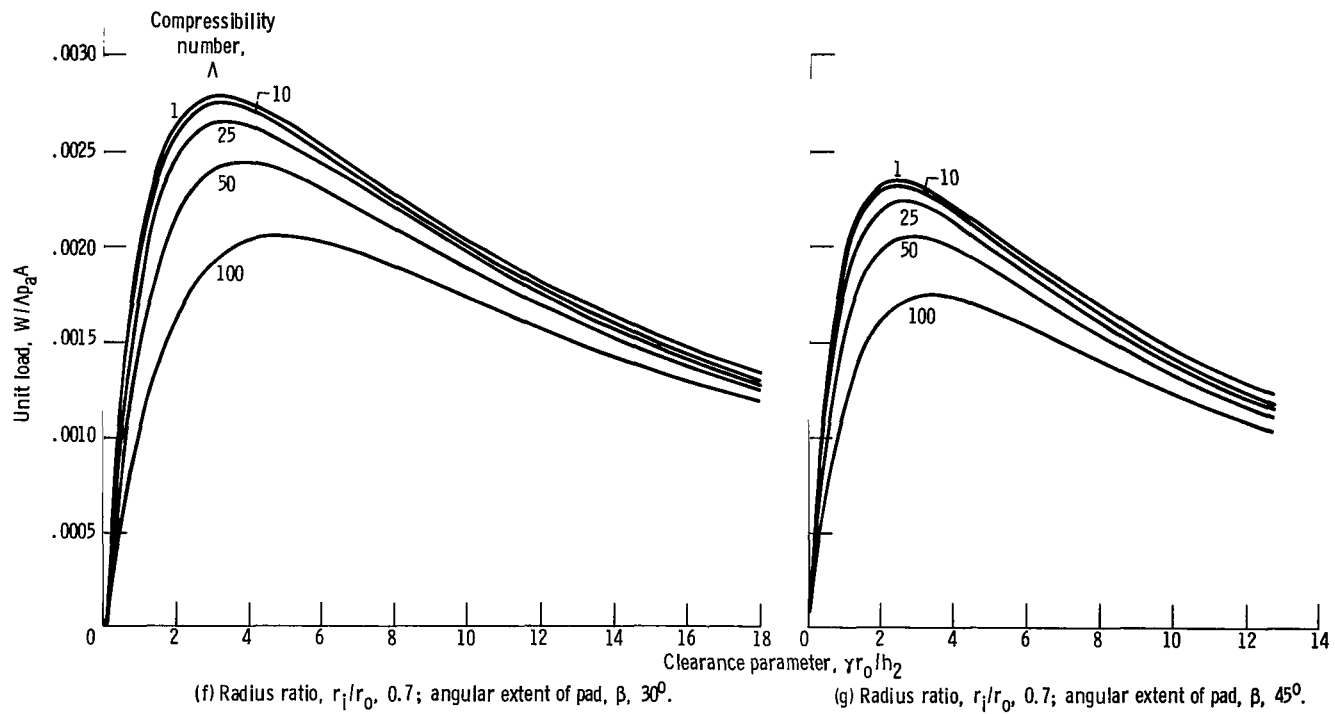


Figure 6. - Concluded.

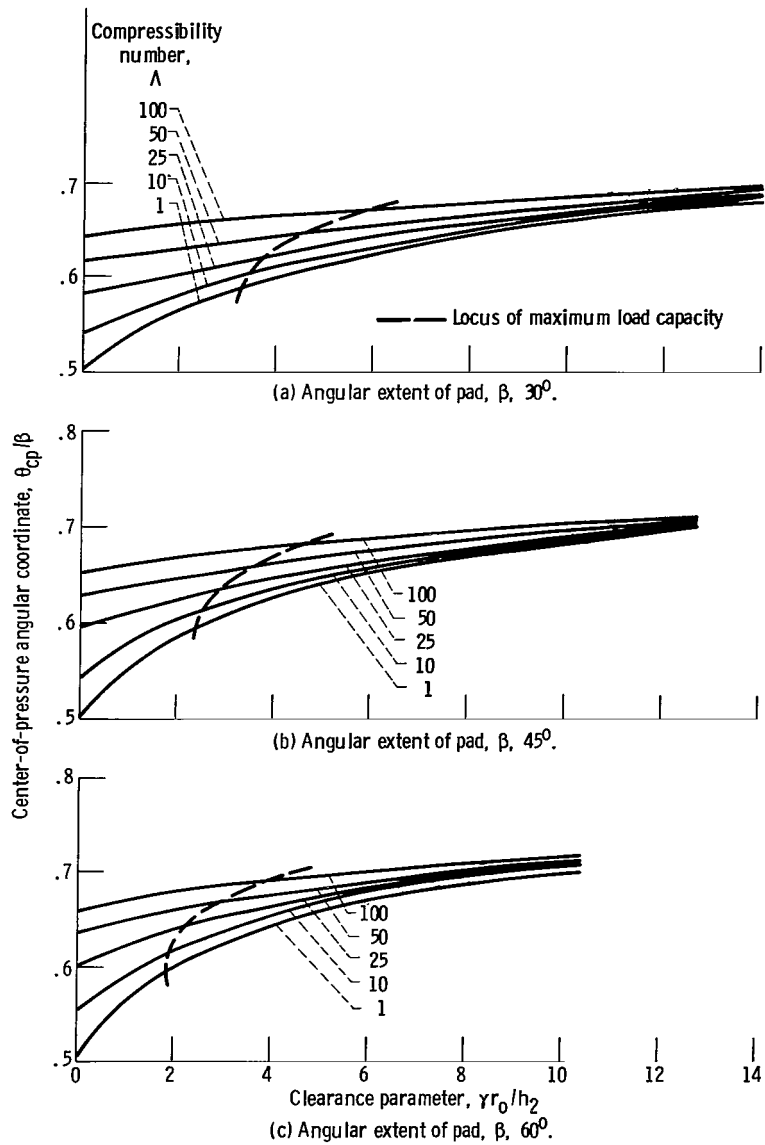


Figure 7. - Angular coordinate of center of pressure for radius ratio of 0.3 and different angular extents of pad at various compressibility numbers.

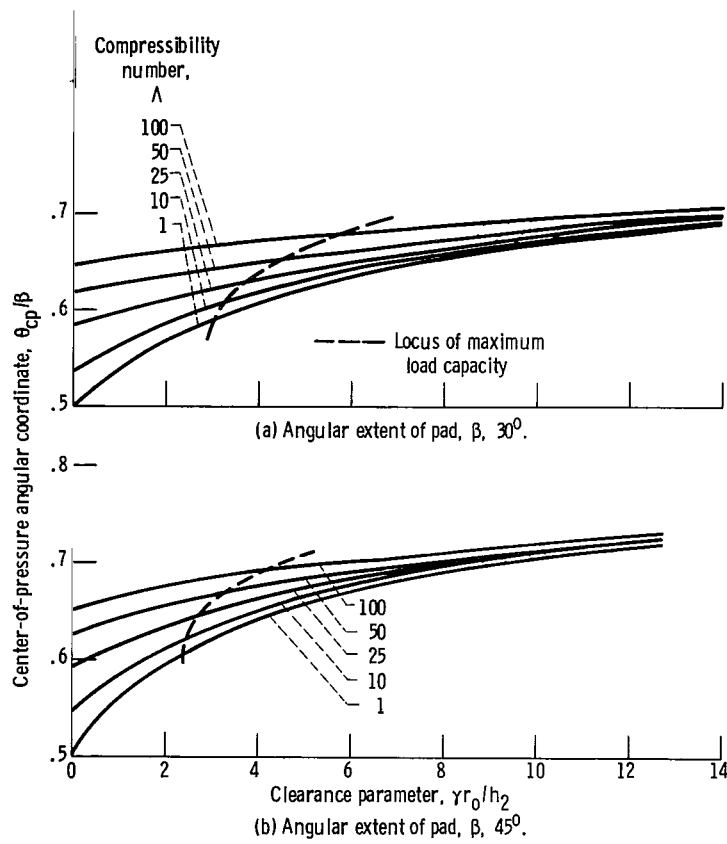


Figure 8. - Angular coordinate of center of pressure for radius ratio of 0.5 and different angular extents of pad at various compressibility numbers.

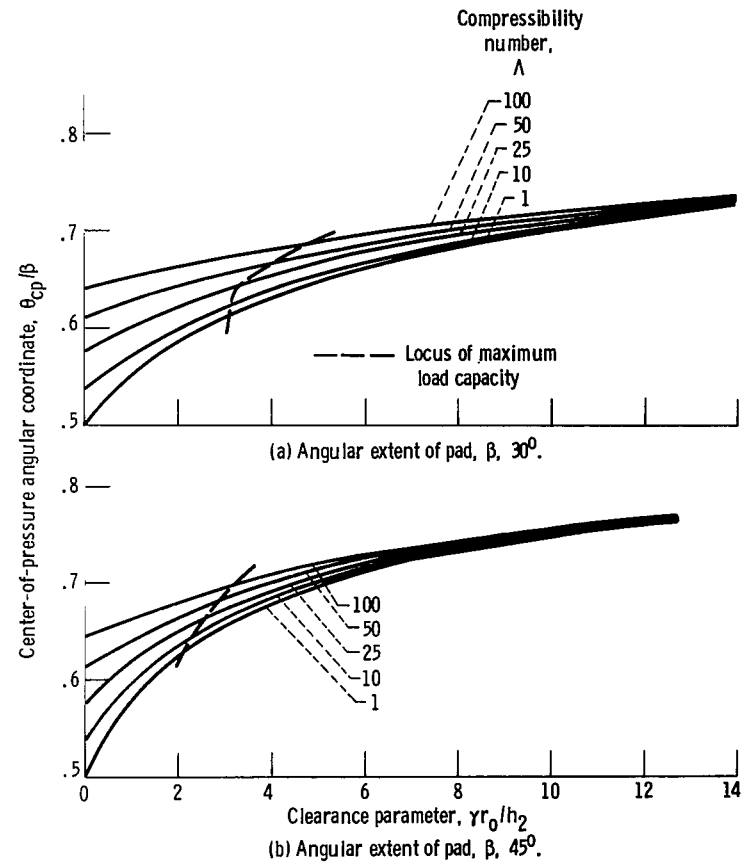


Figure 9. - Angular coordinate of center of pressure for radius ratio of 0.7 and different angular extents of pad at various compressibility numbers.

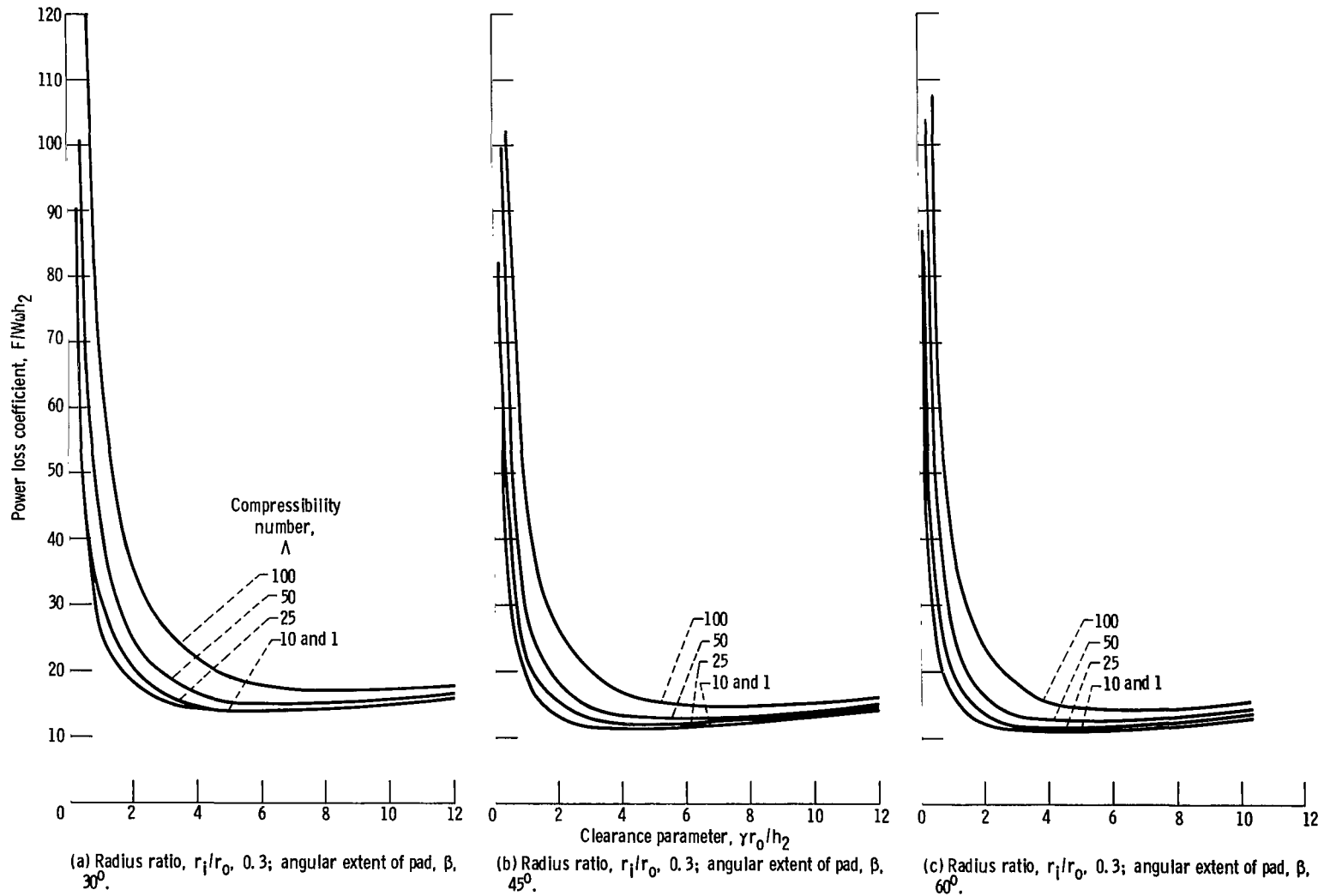


Figure 10. - Power loss coefficient for various radius ratios and angular extents of pad, at various compressibility numbers.

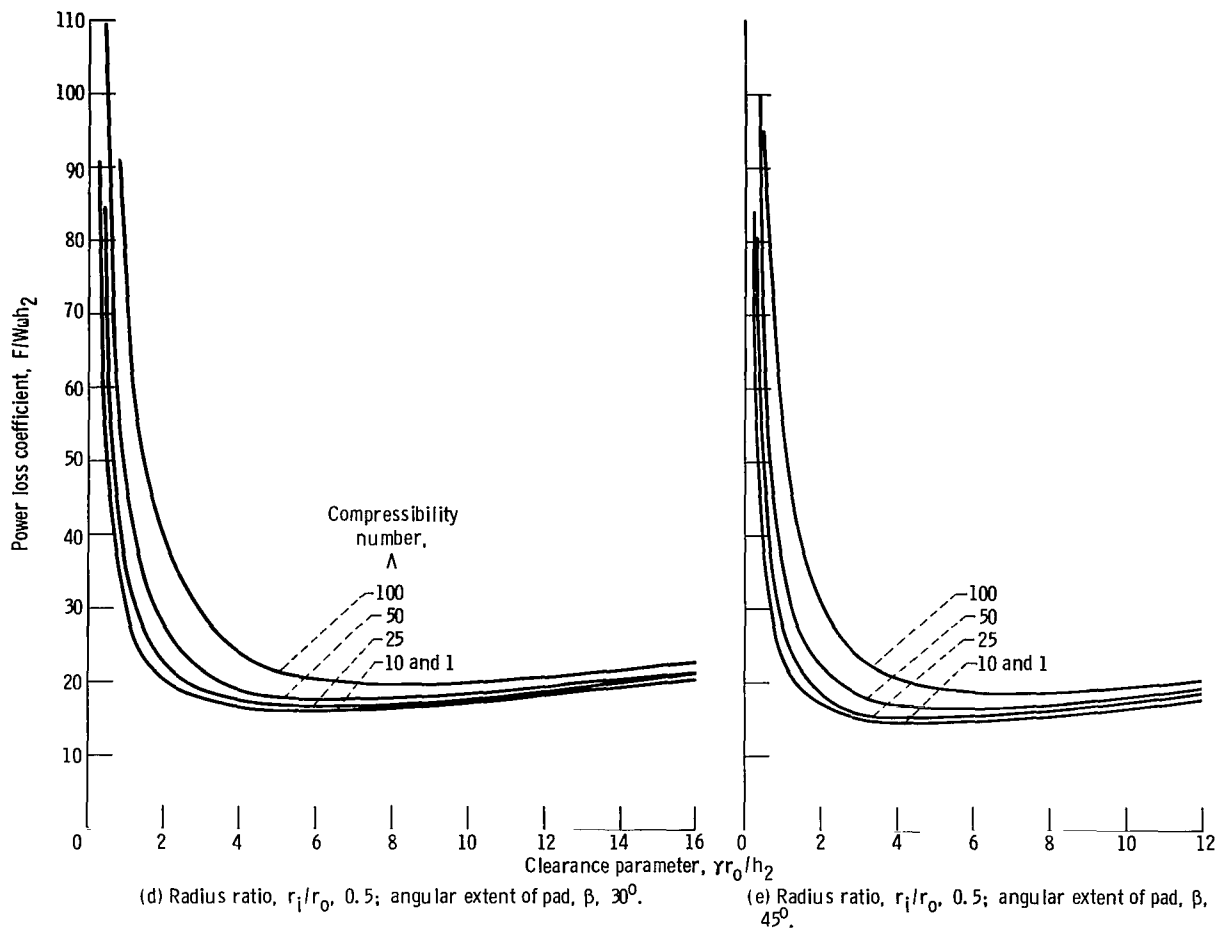
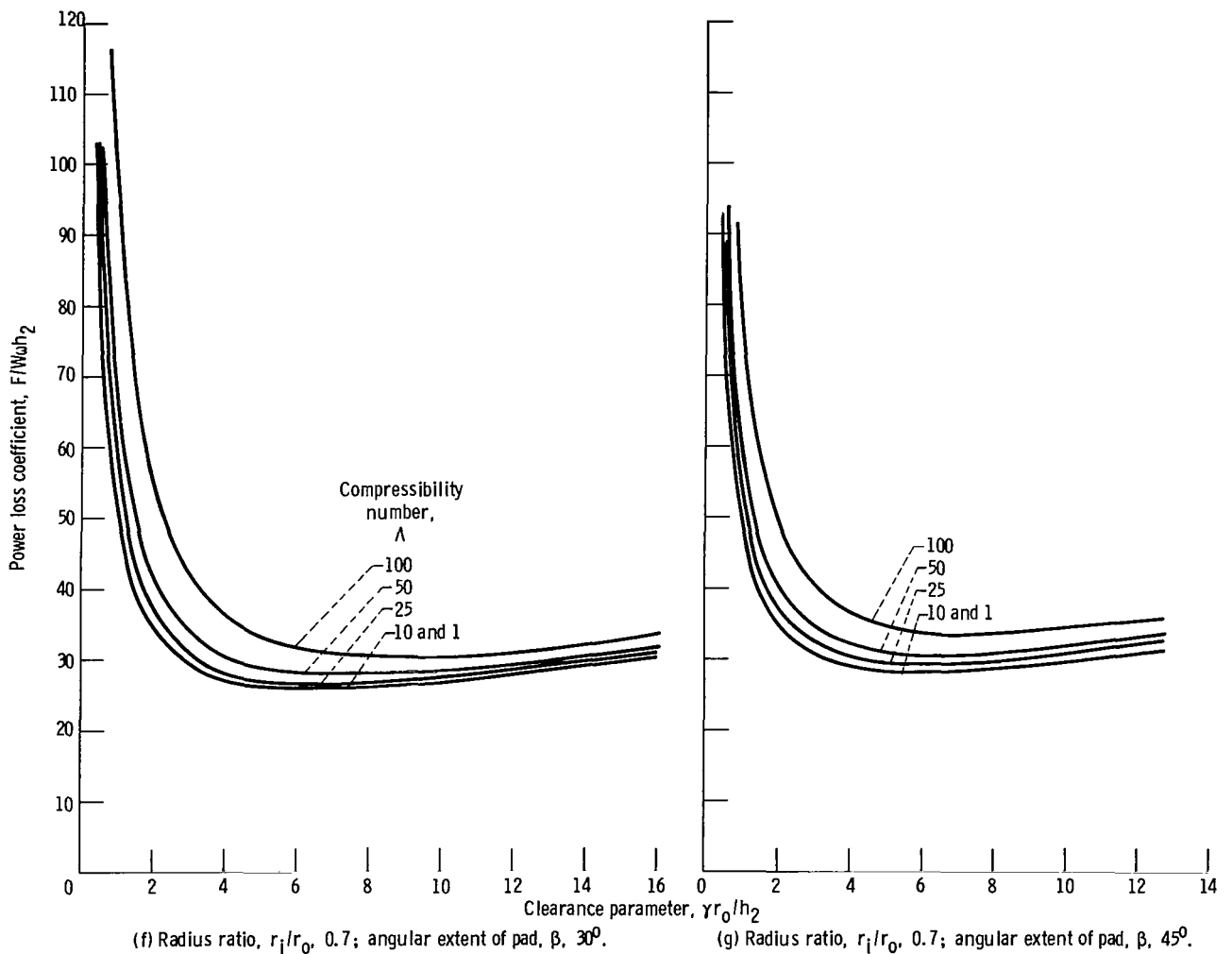


Figure 10. - Continued.



(f) Radius ratio, r_1/r_0 , 0.7; angular extent of pad, β , 30° .

(g) Radius ratio, r_1/r_0 , 0.7; angular extent of pad, β , 45° .

Figure 10. - Concluded.



570 001 C1 U D 760604 S00903DS
DEPT OF THE AIR FORCE
AF WEAPONS LABORATORY
ATTN: TECHNICAL LIBRARY (SUL)
KIRTLAND AFB NM 87117

POSTMASTER: If Undeliverable (Section 158
Postal Manual) Do Not Return

"The aeronautical and space activities of the United States shall be conducted so as to contribute . . . to the expansion of human knowledge of phenomena in the atmosphere and space. The Administration shall provide for the widest practicable and appropriate dissemination of information concerning its activities and the results thereof."

—NATIONAL AERONAUTICS AND SPACE ACT OF 1958

NASA SCIENTIFIC AND TECHNICAL PUBLICATIONS

TECHNICAL REPORTS: Scientific and technical information considered important, complete, and a lasting contribution to existing knowledge.

TECHNICAL NOTES: Information less broad in scope but nevertheless of importance as a contribution to existing knowledge.

TECHNICAL MEMORANDUMS: Information receiving limited distribution because of preliminary data, security classification, or other reasons. Also includes conference proceedings with either limited or unlimited distribution.

CONTRACTOR REPORTS: Scientific and technical information generated under a NASA contract or grant and considered an important contribution to existing knowledge.

TECHNICAL TRANSLATIONS: Information published in a foreign language considered to merit NASA distribution in English.

SPECIAL PUBLICATIONS: Information derived from or of value to NASA activities. Publications include final reports of major projects, monographs, data compilations, handbooks, sourcebooks, and special bibliographies.

TECHNOLOGY UTILIZATION PUBLICATIONS: Information on technology used by NASA that may be of particular interest in commercial and other non-aerospace applications. Publications include Tech Briefs, Technology Utilization Reports and Technology Surveys.

Details on the availability of these publications may be obtained from:

SCIENTIFIC AND TECHNICAL INFORMATION OFFICE

NATIONAL AERONAUTICS AND SPACE ADMINISTRATION

Washington, D.C. 20546